Heat Transfer Research 47(7), 633–651 (2016)

ULTRAFAST RADIATIVE TRANSFER CHARACTERISTICS IN MULTILAYER INHOMOGENEOUS 3D MEDIA SUBJECTED TO A COLLIMATED SHORT SQUARE PULSE TRAIN

Masato Akamatsu[1,*] *& Zhixiong Guo*[2]

[1]*Graduate School of Science and Engineering, Yamagata University, 4-3-16 Jonan, Yonezawa, Yamagata 992-8510, Japan*

[2]*Department of Mechanical and Aerospace Engineering, Rutgers, The State University of New Jersey, Piscataway, NJ 08854, USA*

*Address all correspondence to: M. Akamatsu; E-mail: akamatsu@yz.yamagata-u.ac.jp

We carried out 3D numerical modeling to understand ultrafast radiative transfer characteristics in multilayer inhomogeneous media, irradiated by a collimated short square pulse train, using the discrete-ordinates method (DOM) in combination with Duhamel's superposition theorem. The DOM was used to first obtain the temporal solution subjected to a single unit step pulse. Duhamel's superposition theorem was then used to reconstruct the response to different kinds of pulse trains. The efficiency of superposition was shown via CPU time comparison with and without use of superposition. The reflectance and transmittance signals are characterized, focusing on the effects of optical thickness, scattering albedo, pulse width and interval, and detection position.

KEY WORDS: *discrete-ordinates method, superposition, short pulse, radiative transfer, inhomogeneous media*

1. INTRODUCTION

The advent of ultrafast lasers has brought many new applications, in particular in biomedicines and material processing, such as laser tissue ablation (Huang and Guo, 2010; Jiao and Guo, 2011), laser tissue soldering and welding (Kim and Guo, 2004), protein shock (Sajjadi et al., 2013), thermal response (Jiao and Guo, 2009), and the detection of tumors by using an exogenous fluorescence agent and ultrashort near-infrared laser pulses (Quan and Guo, 2004).

The development of optical computed tomography (optical-CT) has been proceeding vigorously, as the optical-CT is expected to obtain imaging information on the physiology as well as morphology inside living bodies (Yamada, 1995; Hebden et al., 2001). To realize a fully functional optical-CT, better understanding of the characteristics of laser radiative transfer of scattered signals in highly scattering and weakly absorbing biological tissues is needed. It is important that accurate solutions be obtained for the equation of radiative transfer. There have been many proposed numerical methods to solve the hyperbolic equation of ultrafast radiative transfer accurately as recently reviewed by Guo and Hunter (2013). The solution based on the frequency-domain diffusion approximation was also considered (Liu and Liu, 2012).

Some prior numerical studies relevant to the present study are reviewed as follows. Muthukumaran and Mishra (2008b,c,d) concentrated on numerical studies for elucidating the radiative transfer characteristics in a homogeneous medium and a participating medium consisting of local inhomogeneity subjected to a diffuse or a collimated pulse train consisting of 1–4 pulses with a step or Gaussian temporal variation, using the fi-

1064-2285/16/$35.00

NOMENCLATURE

c	speed of light	**Greek symbols**	
d_c	width of the collimated laser sheet	δ	Dirac delta function
$f(t)$	boundary condition function	Δt	time step
I	radiation intensity	Δx, Δy, Δz	grid size
I_c	laser intensity	Φ	scattering phase function
I_p	radiation intensity at the node of a control volume	γ	weighting factor
		η, μ, ξ	direction cosines
L	length of a cube	ρ	diffuse reflectivity
N	angular discrete order in S_N approximation	σ_a	absorption coefficient
		σ_e	extinction coefficient
n	number of angular discretization	σ_s	scattering coefficient
Q	net radiative heat flux	τ	optical thickness
R	reflectance	ω	scattering albedo
$\vec{r}$	position vector	**Subscripts**	
S	source term		
$\hat{s}$	discrete ordinate direction	b	blackbody value
T	transmittance	c	collimated laser
t	time	d	downstream surface
t^*	nondimensional time = ct/L	p	control volume index
t_d	pulse interval	u	upstream surface
t_p	pulse width	w	wall
$U(t)$	unit step function	**Superscripts**	
w	angular weight		
x, y, z	Cartesian coordinates	l	discrete direction index
x^*, y^*, z^*	nondimensional coordinates	*	dimensionless quantity

nite volume method (FVM). Muthukumaran and Mishra (2008a) investigated the temporal transmittance and reflectance signals on a 1D inhomogeneous medium consisting of 2–3 layers subjected to a single step laser pulse or a train of four step pulses with a pulse train interval that is the same as the pulse width. Muthukumaran et al. (2011) analyzed signals originating from a human tissue phantom subjected to a short-pulse laser that can have a temporal span of the order of a nano-, pico-, or a femtosecond with both step and Gaussian distributions, to assess the case of a human skin-mimic tissue. Mishra et al. (2012) compared temporal signals resulting from the boundary conditions of a train of pulses by using both the FVM and the DOM for various optical situations, and they found that the solutions computed using the FVM were in good agreement with those computed using the DOM. However, this group of authors used "direct pulse simulation" (Mishra et al.,

2006) to model pulse train irradiation, i.e., they computed radiative transfer using the aforementioned methods (FVM or DOM) from the start until the end of the pulse train. In such a situation, the numerical errors accumulated with time advance are obvious and the CPU times used is a simple product of the CPU time for a single pulse and the pulse numbers in a pulse train.

Recently, Yi et al. (2013) developed a MC model with a combination of time shift and superposition principle for solving transient vector radiative transfer in a scattering layer. Zhang et al. (2013, 2014a) solved transient radiative transfer problem in a 1D slab containing absorbing and scattering media subjected to a short laser irradiation using the lattice Boltzmann method (LBM). Zhang et al. (2014b) solved transient radiative transfer in 2D semitransparent media subjected to a collimated short laser irradiation by the natural element method (NEM). Padhi et al. (2011) employed the CLAM scheme for discretizing the spatial term. Huang et al. (2009) investigated the transient radiative transfer process within absorbing, scattering, and nonemitting two-layer participating media by using the DRESOR method based on the Monte Carlo (MC) method to clarify the dual-peak phenomenon of a temporal reflectance signal and the existence conditions of the dual peak.

For analyzing ultrafast radiative transfer in a participating medium imposed by a laser pulse, Guo and Kumar (2002) were the first to find that Duhamel's superposition theorem can be used to construct the pulsed radiation response subjected to various incident pulse shapes based on the results of a unit step pulse, since the transient radiative transfer equation is linear when medium emission is negligible within an ultrashort timescale. Liu and Hsu (2008) followed this superposition in the consideration of time shifts in a 1D purely scattering medium subjected to a square pulse irradiation train.

Akamatsu and Guo (2011, 2013b) conducted complete transient 3D numerical computations by applying the DOM and Duhamel's superposition theorem to scrutinize the radiative transfer characteristics in a homogeneous medium subjected to a diffuse or a collimated short square pulse train consisting of five or 10 pulses. They found that the superposition effect for transmitted pulse trains strongly depends on the pulse train interval between two successive pulses and the pulse broadening under diffuse and collimated irradiations. They also elucidated that Duhamel's superposition theorem provides better accuracy and computational efficiency than the direct pulse simulation for the radiative transfer analysis of multiple pulses, because Duhamel's superposition theorem needs only one solution exposed to a single unit step square pulse for different problems subjected to a square pulse train with various pulse widths and pulse train intervals, whereas the direct pulse simulation is time-consuming and subject to increased numerical errors because of error accumulation (Akamatsu and Guo, 2013a).

In the real world of laser-matter interactions, the medium properties are generally inhomogeneous. Thus, the investigation and elucidation of ultrafast radiative transfer characteristics in inhomogeneous participating media subjected to a pulse train are very important to advance the applications of ultrafast laser technology. To this end, we carried out the complete transient 3D numerical computations in this study to understand the ultrafast radiative transfer characteristics in inhomogeneous participating media. We considered a medium of three layers of different properties, which is subjected to a collimated short square pulse train; and solved the problem by combining the DOM and Duhamel's superposition theorem. The effects of the pulse width, pulse interval, scattering albedo, optical thickness, and detecting position on the reflectance and transmittance signals were scrutinized.

2. GOVERNING EQUATIONS

In the present numerical computations, a cube of three different participating layers with uniform extinction coefficient was considered. The geometry of the model is shown in Fig. 1a. The collimated laser sheet direct-

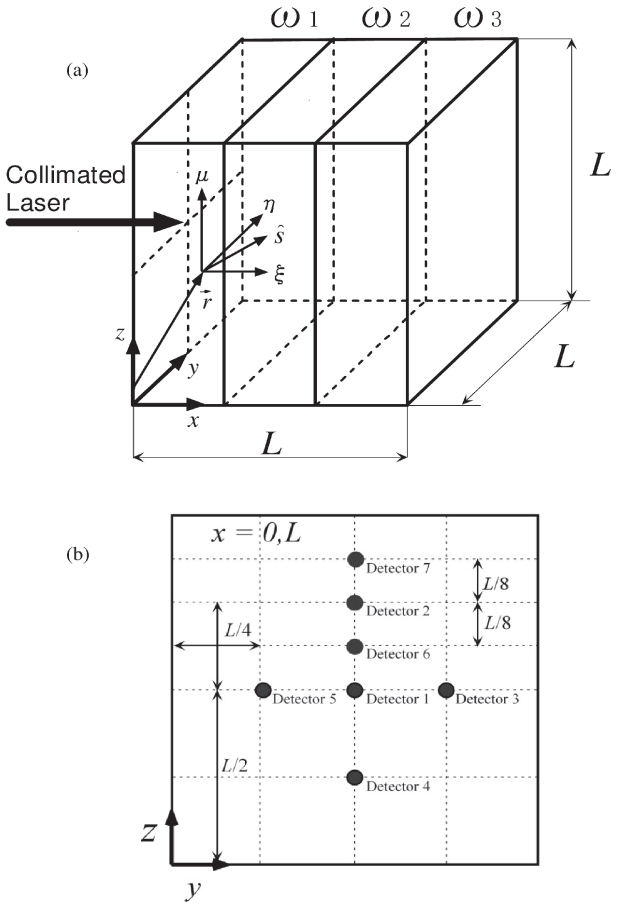

FIG. 1: (a) 3D geometry and (b) the locations of detectors 1–7 in the *y*–*z* plane at $x = 0$ and L

ed to the wall is normally incident at the center spot in the plane at $x = 0$ with a width of d_c, and $d_c = L/49$. The temporal variation of the pulse is a step function. As seen in Fig. 1b, the reflected signals were detected at locations 2–7 at the wall of $x = 0$, and the transmitted signals were detected at locations 1–7 at the opposite wall of $x = L$. The participating medium is assumed to be cold (neglecting emission).

The transient equations of diffuse radiative transfer in discrete ordinates can be formulated as

$$\frac{1}{c}\frac{\partial I^l}{\partial t} + \xi^l \frac{\partial I^l}{\partial x} + \eta^l \frac{\partial I^l}{\partial y} + \mu^l \frac{\partial I^l}{\partial z} + \sigma_e I^l = \sigma_e S^l \ , \qquad l = 1, 2, \ldots, n \ . \tag{1}$$

The extinction coefficient σ_e is the summation of the absorption coefficient σ_a and scattering coefficient σ_s. The scattering albedo is $\omega = \sigma_s/\sigma_e$. The radiative source term S^l, neglecting blackbody emission, can be expressed as

$$S^l = \frac{\omega}{4\pi} \sum_{i=1}^{n} w^i \Phi^{il} I^i + S_c^l \ , \qquad l = 1, 2, \ldots, n \ . \tag{2}$$

The first term on the right-hand side in Eq. (2) is the contribution of in-scattering radiation intensities from all discrete ordinate directions. The quantity $\Phi(\hat{s}^i \rightarrow \hat{s}^l)$ is the scattering phase function. In the present study, the scattering is assumed to be isotropic or scaled isotropic (Guo and Maruyama, 1999). The second term is the source contribution of the collimated laser irradiation, which is the driving force of the scattered radiation propagation and transport in the medium:

$$S_c^l = \frac{\omega}{4\pi} I_c \Phi \left(\xi^c \xi^l + \eta^c \eta^l + \mu^c \mu^l \right), \tag{3}$$

where (ξ^c, η^c, μ^c) represents the collimated laser incident direction. In the present model, $\xi^c = 1$, $\eta^c = 0$, and $\mu^c = 0$, since the collimated laser is normally incident at the wall at $x = 0$, as shown in Fig. 1a.

The collimated laser intensity (heat flux) is distributed inside the medium as

$$I_c \left(x, y, z, \xi^c, t \right) = I_0 \left(x = 0, y = z = \frac{L}{2}, t - \frac{x}{c\xi^c} \right) e^{-\frac{\sigma_e x}{\xi^c}} \delta \left(\xi^c - 1 \right), \tag{4}$$

in which δ is the Dirac delta function and I_0 is the laser beam heat flux irradiated onto the surface of the medium (the surface reflection is deducted). In the region where no collimated laser irradiation passes through, $I_c = S_c = 0$.

A quadrature set of the DOM S_N-approximation includes n discrete ordinates with appropriate angular weight, in which $n = N(N+2)$. In the present computations, the S_{12}-approximation is applied for obtaining the solution for the basic problem in which a cubic participating medium is exposed to collimated irradiation of a single unit step square pulse.

The walls are assumed to be gray and diffusely reflecting. For example, the diffuse intensity at the wall of $x = 0$ is

$$I_w = (1 - \rho) I_{bw} + \frac{\rho}{\pi} \sum_{\xi^l < 0}^{n/2} w^l I^l \left| \xi^l \right|, \tag{5}$$

where I_w is the diffuse intensity at the wall, I_{bw} is the blackbody intensity at the wall, ρ is the diffuse reflectivity of the wall surface, and $n/2$ denotes that one-half of the n different intensities emanates from the wall. Similarly, the relationships for the remaining five walls can be set up. In the present numerical computations, the diffuse reflectivity of the wall surface is $\rho = 0$; that is, the sidewalls are black and absorb all incident radiation.

Once the intensities have been determined, the net radiative heat fluxes Q_x, Q_y, and Q_z are evaluated from

$$Q_x = \sum_{l=1}^{n} \xi^l w^l I^l + I_c, \; Q_y = \sum_{l=1}^{n} \eta^l w^l I^l, \; Q_z = \sum_{l=1}^{n} \mu^l w^l I^l. \tag{6}$$

The transient reflectance at $x = 0$ and the transient transmittance at the opposite output wall of $x = L$ for the basic problem are defined as

$$R(x = 0, y, z, t) = \frac{Q_x(x = 0, y, z, t) - I_c(x = 0, y, z, t)}{I_0}, \tag{7}$$

$$T(x = L, y, z, t) = \frac{Q_x(x = L, y, z, t)}{I_0}. \tag{8}$$

3. NUMERICAL SCHEME

In our previous numerical investigation (Akamatsu and Guo, 2011), we examined the influences of the spatial grid and time step on the temporal profiles of reflectance and transmittance to minimize the effects of false radiation propagation and numerical diffusion for solving ultrafast radiative transfer in a highly scattering medium, and the optimum spatial grid and time step were decided. In the present numerical computations, the spatial grid and time step determined in the previous study were also adopted. Namely, the spatial grid number and the time step were $49 \times 49 \times 49$ and $\Delta t^* = 0.006$, respectively.

The control volume approach is used for the spatial discretization to solve the transient radiation transfer equation, i.e., Eq. (1). In each control volume, Eq. (1) is discretized temporally and spatially. The final discretization equation for the cell intensity in a generalized form (Guo and Kumar, 2002) becomes

$$I_P^l = \frac{\dfrac{1}{c\Delta t} I_p^{l0} + \sigma_e S_p^l + \dfrac{\left|\xi^l\right|}{\gamma_x^l \Delta x} I_{xu}^l + \dfrac{\left|\eta^l\right|}{\gamma_y^l \Delta y} I_{yu}^l + \dfrac{\left|\mu^l\right|}{\gamma_z^l \Delta z} I_{zu}^l}{\dfrac{1}{c\Delta t} + \sigma_e + \dfrac{\left|\xi^l\right|}{\gamma_x^l \Delta x} + \dfrac{\left|\eta^l\right|}{\gamma_y^l \Delta y} + \dfrac{\left|\mu^l\right|}{\gamma_z^l \Delta z}}, \tag{9}$$

where I_p is the intensity at the node of a control volume, I_p^{l0} is the intensity at the previous time step, and I_{xu}^l, I_{yu}^l, and I_{zu}^l are the radiation intensities on the upstream surface in the $\hat{s}^l$ direction. In the present method, the positive scheme proposed by Lathrop (1969) is applied to determine the values of weighting factors γ_x^l, γ_y^l, and γ_z^l. With the nodal intensity obtained from Eq. (9), the unknown radiation intensities on the downstream surface in the same direction are computed as follows:

$$I_p^l = \gamma_x^l I_{xd}^l + (1 - \gamma_x^l) I_{xu}^l = \gamma_y^l I_{yd}^l + (1 - \gamma_y^l) I_{yu}^l = \gamma_z^l I_{zd}^l + (1 - \gamma_z^l) I_{zu}^l, \tag{10}$$

where I_{xd}^l, I_{yd}^l, and I_{zd}^l are the radiation intensities on the downstream surface in the $\hat{s}^l$ direction. The derivation of Eq. (10) is well described by Modest (2003) for the steady-state situation.

In Eq. (9), the traveling distance $c\Delta t$ should not exceed the control volume spatial step, i.e., $c\Delta t < \min\{\Delta x, \Delta y, \Delta z\}$. This is because a light beam always travels at the speed of light c in the medium. Hence, the following condition is imposed to eliminate the numerical diffusion (Guo and Kumar, 2001):

$$\Delta t^* < \min\{\Delta x^*, \Delta y^*, \Delta z^*\}. \tag{11}$$

We verified the present method by comparison with the existing published results and/or with the Monte Carlo simulation for a variety of example problems in 2D and 3D systems (Guo and Kumar, 2001, 2002). We found that the present method was accurate and efficient.

4. SUPERPOSITION FOR A PULSE TRAIN

In the present computations, Duhamel's theorem is used to construct the responses when a cold medium is subjected to a pulse train instead of direct pulse simulation. Duhamel's theorem relates the solution $\Theta(\vec{r}, t)$ of a problem subjected to the time-dependent boundary condition of the function $f(t)$ to the solution $\theta(\vec{r}, t)$ of a corresponding basic problem as (Ozisik, 1993):

$$\Theta(\vec{r}, t) = \sum_j \theta(\vec{r}, t - \tau_j) \Delta f_j U(t - \tau_j) + \int_{\tau=0}^{t} \theta(\vec{r}, t - \tau) f'(\tau) d\tau. \tag{12}$$

In this equation Δf_j is the step change occurring at time τ_j, and $U(t - \tau_j)$ is the unit step function. For example, if the boundary is subjected to a pulse train consisting of five square pulses with the pulse width t_p and the time interval t_d between the two successive pulses, Eq. (12) can be simplified as

$$\begin{aligned}\Theta(\vec{r}, t) &= \theta(\vec{r}, t) - \theta(\vec{r}, t - t_p) \\ &+ \theta(\vec{r}, t - t_p - t_d) - \theta(\vec{r}, t - 2t_p - t_d) \\ &+ \theta(\vec{r}, t - 2t_p - 2t_d) - \theta(\vec{r}, t - 3t_p - 2t_d) \\ &+ \theta(\vec{r}, t - 3t_p - 3t_d) - \theta(\vec{r}, t - 4t_p - 3t_d) \\ &+ \theta(\vec{r}, t - 4t_p - 4t_d) - \theta(\vec{r}, t - 5t_p - 4t_d)\,.\end{aligned} \tag{13}$$

Figure 2a shows the temporal profiles of the transmittance at detector 1 in the homogeneous and inhomogeneous media, respectively, subjected to a single diffuse unit step square pulse. Here, the unit cube has one

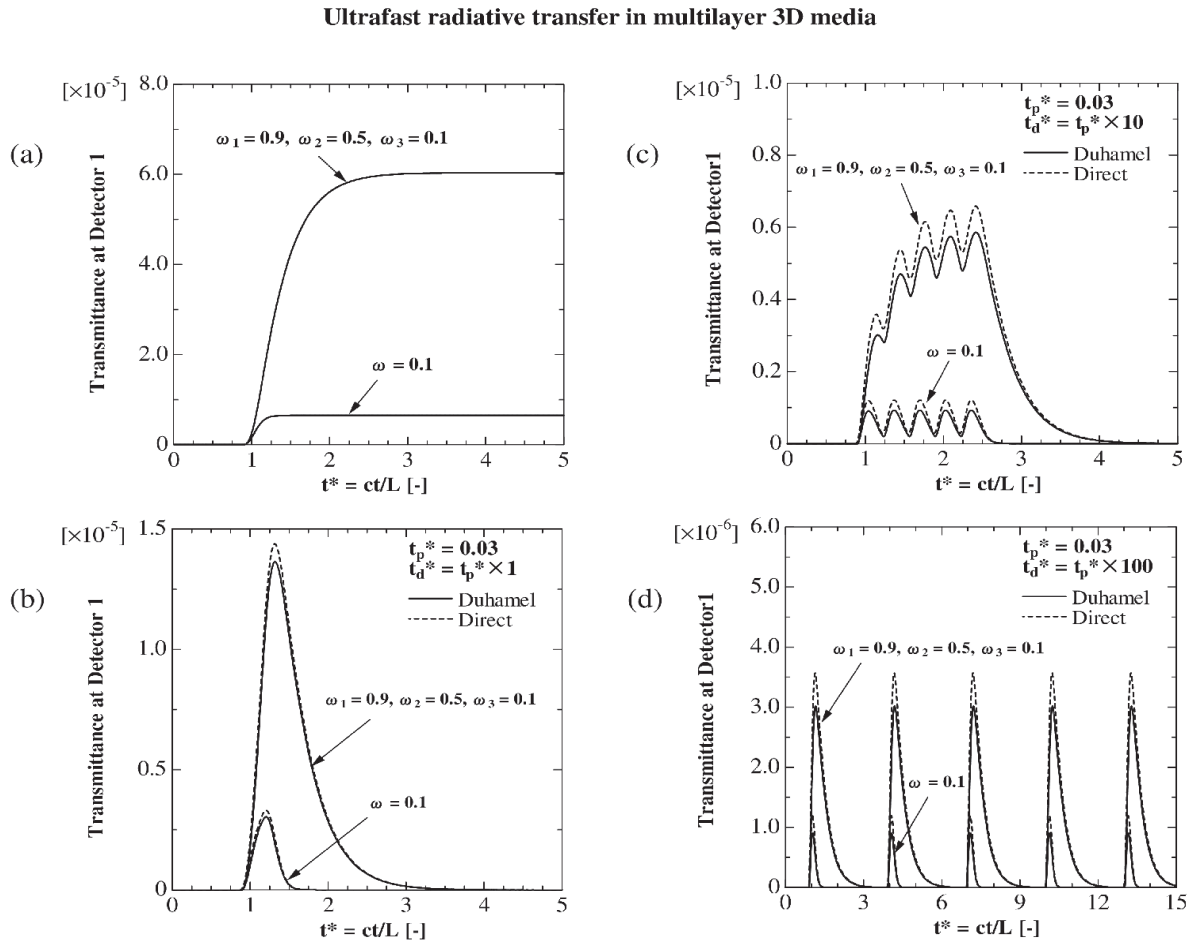

FIG. 2: Temporal profiles of the transmittance detected by detector 1 in the homogeneous and inhomogeneous media with one hot wall: a) single diffuse unit step square pulse, b–d) diffuse square pulse train consisting of five pulses with constant pulse width

hot wall at $x^* = 0$. For the homogeneous medium, its optical thickness is $\sigma_e L = 10$ and $\omega = 0.1$. The three layers in the inhomogeneous medium have same optical thickness 10/3 for each layer with the values $\omega_1 = 0.9$, $\omega_2 = 0.5$, $\omega_3 = 0.1$, respectively. For both media, the transmitted pulse computed by the DOM reached a constant value at the long time stage. In Fig. 2b–d, the solid lines show the transmittance signals in the homogeneous and inhomogeneous media subjected to a diffuse square pulse train consisting of five pulses with pulse width $t_p^* = 0.03$ computed by Duhamel's theorem based on the solutions of the basic problem shown in Fig. 2a. The dashed lines show those computed in the direct pulse simulation using the DOM. It is seen that although the transmittances in homogeneous and inhomogeneous media computed by Duhamel's theorem were almost in agreement with those computed by the direct pulse simulation qualitatively, the magnitudes predicted by the two methods did not match quantitatively for the three different pulse intervals, i.e., (b) $t_d^* = t_p^*$, (c) $t_d^* = 10t_p^*$, and (d) $t_d^* = 100t_p^*$. In previous studies for homogeneous media (Akamatsu and Guo, 2011, 2013a,b), it was found that the overlap effect of the pulse train strongly depends on the pulse interval and the magnitude of the pulse broadening. The present study with inhomogeneous media also confirms this dependence.

The computer used for the present calculations was a workstation with an Intel Dual CPU 16 Core Xeon 3.1GHz processor and 32 GB of RAM. The Intel Visual Fortran Composer XE 2011 was used as a compiler. For the transmittances shown in Fig. 2a, the CPU time was 55,188 s to compute the response to one single pulse in the time range from $t^* = 0$ to $t^* = 5$ via the DOM, whereas the transmittances of multiple pulses in Fig. 2b–d computed by Duhamel's superposition based on the solution shown in Fig. 2a were obtained in several seconds. For comparison, for the transmittance of three pulses shown in Fig. 2d using DOM without superposition, the CPU time was 175,271 s to compute from $t^* = 0$ to $t^* = 15$, three times longer than that using the combined method of a base solution and superposition.

The results in Fig. 2 demonstrated again that superposition provides better computational efficiency than the direct pulse simulation for predicting ultrafast radiative transfer of pulse train irradiation, because the superposition needs only one solution exposed to a single unit step square pulse for different problems subjected to a pulse train with various pulse widths and pulse intervals, whereas the direct pulse simulation is time-consuming and subject to increased numerical errors because of error accumulation. Superposition will also provide better accuracy because numerical errors will not be accumulated with addition of extra pulses.

5. RESULTS AND DISCUSSION

In the following, six different media named as Types A, A', A'' and B, B', B'' are considered and their optical properties are listed in Table 1. Types A and B are two homogeneous media with different scattering albedos. The other four types are inhomogeneous media consisted of three layers. The mismatch of refractive indices between different layers was neglected.

Figure 3 shows the temporal profiles of the reflectance and transmittance of six media subjected to a single collimated unit step square pulse computed by DOM with S_{12} scheme. In Figs. 3a and 3d, the steady-state reflectances detected by detector 6 for the inhomogeneous media Types A' ($\omega_1 = 0.9$, $\omega_2 = 0.5$, $\omega_3 = 0.1$) and B' ($\omega_1 = 0.1$, $\omega_2 = 0.5$, $\omega_3 = 0.9$) shown by the solid lines were almost the same as those for the respective homogeneous medium Types A ($\omega = 0.9$) and B ($\omega = 0.1$) shown by the dashed lines.

However, those for Types A'' and B'' with a thin first layer clearly differed from those for Types A' and B'. As the position of detector recedes from detector 6, the detected reflectance for Types A' and B' decreased remarkably. The reflectance detected by detector 7 for Types A' and B' was 0.038 times and 0.0026 times of those detected by detector 6 for Types A' and B', respectively. We found that the reflectance signal depends

TABLE 1: The optical thicknesses and scattering albedos for different media

	Medium type					
	A	**A'**	**A"**	**B**	**B'**	**B"**
First layer	$\sigma_e L = 10$ $\omega = 0.9$	$\tau_1 = \frac{10}{3}$ $\omega_1 = 0.9$	$\tau_1 = \frac{10}{7}$ $\omega_1 = 0.9$	$\sigma_e L = 10$ $\omega = 0.1$	$\tau_1 = \frac{10}{3}$ $\omega_1 = 0.1$	$\tau_1 = \frac{10}{7}$ $\omega_1 = 0.1$
Second layer		$\tau_2 = \frac{10}{3}$ $\omega_2 = 0.5$	$\tau_2 = \frac{20}{7}$ $\omega_2 = 0.5$		$\tau_2 = \frac{10}{3}$ $\omega_2 = 0.5$	$\tau_2 = \frac{20}{7}$ $\omega_2 = 0.5$
Third layer		$\tau_3 = \frac{10}{3}$ $\omega_3 = 0.1$	$\tau_3 = \frac{40}{7}$ $\omega_3 = 0.1$		$\tau_3 = \frac{10}{3}$ $\omega_3 = 0.9$	$\tau_3 = \frac{40}{7}$ $\omega_3 = 0.9$

strongly on the detecting position and the optical property of the first layer and the effects of the second layer become significant when the first layer is optically thin.

In Fig. 3b, the transmittance detected by detector 1 for Type A' almost agreed with those for Types B and A". However, that for Type A was 1.12 times larger than that for Type A'. In Fig. 3e, the transmittances detected by detector 1 for Types A, B, B', and B" were slightly different; that for Type A was 1.05 times of that for Type B'; and that for Type B was 0.94 times of that for Type B'. In Fig. 3c, the transmittances detected by detectors 2–7 in the inhomogeneous media for Types A' and A" were larger than that detected by detector 6 in the homogeneous medium with a highly absorbing characteristic for Type B, whose scattering albedo is the same as that of the third layer for Types A' and A". For Type A', the transmittances detected by detectors 2 and 7 were 0.59 times and 0.36 times of that detected by detector 6, respectively. On the other hand, the transmittances detected by detector 6 for Types A" and B was 0.27 times and 0.11 times of that detected by detector 6 for Type A'. In Fig. 3f, the transmittance detected by detectors 2–7 in the inhomogeneous medium for Types B' and B" were smaller than that detected by detector 6 in the homogeneous medium with the highly scattering characteristic for Type A, whose scattering albedo is the same as the third layer for Types B' and B". For Type B', the transmittances detected by detectors 2 and 7 were 0.36 times and 0.14 times of that detected by detector 6, respectively. The transmittances detected by detector 6 for Types B" and A were 2.1 times and 6.3 times of that detected by detector 6 for Type B'.

Figures 4–9 show the temporal profiles of the reflectance and transmittance in the homogeneous and inhomogeneous participating media subjected to a single collimated square pulse and a collimated square pulse train consisting of five pulses reconstructed by Duhamel's theorem based on the basic solutions computed by the DOM for a simple step pulse with results shown in Fig. 3.

The transient responses of reflectance for the pulse width of $t_p^* = 0.03$ and the pulse train intervals of $t_d^* = t_p^*$, 10 t_p^* are plotted in Fig. 4, and those for the pulse width of $t_p^* = 0.3$ are shown in Fig. 5. The figures in the left column are the reflectance detected by detector 6 for Types A, A', and A", respectively; and those in the right column are those detected by detector 6 for Types B, B', and B". The Type A model is a homogeneous medium with a high scattering property which is identical to the first layer of Types A' and A". The Type B model is also a homogeneous medium with a high absorbing property identical to the first layer of Types B' and B". The reflectance signals subjected to a single square pulse shown in Figs. 4a,d and 5a,d

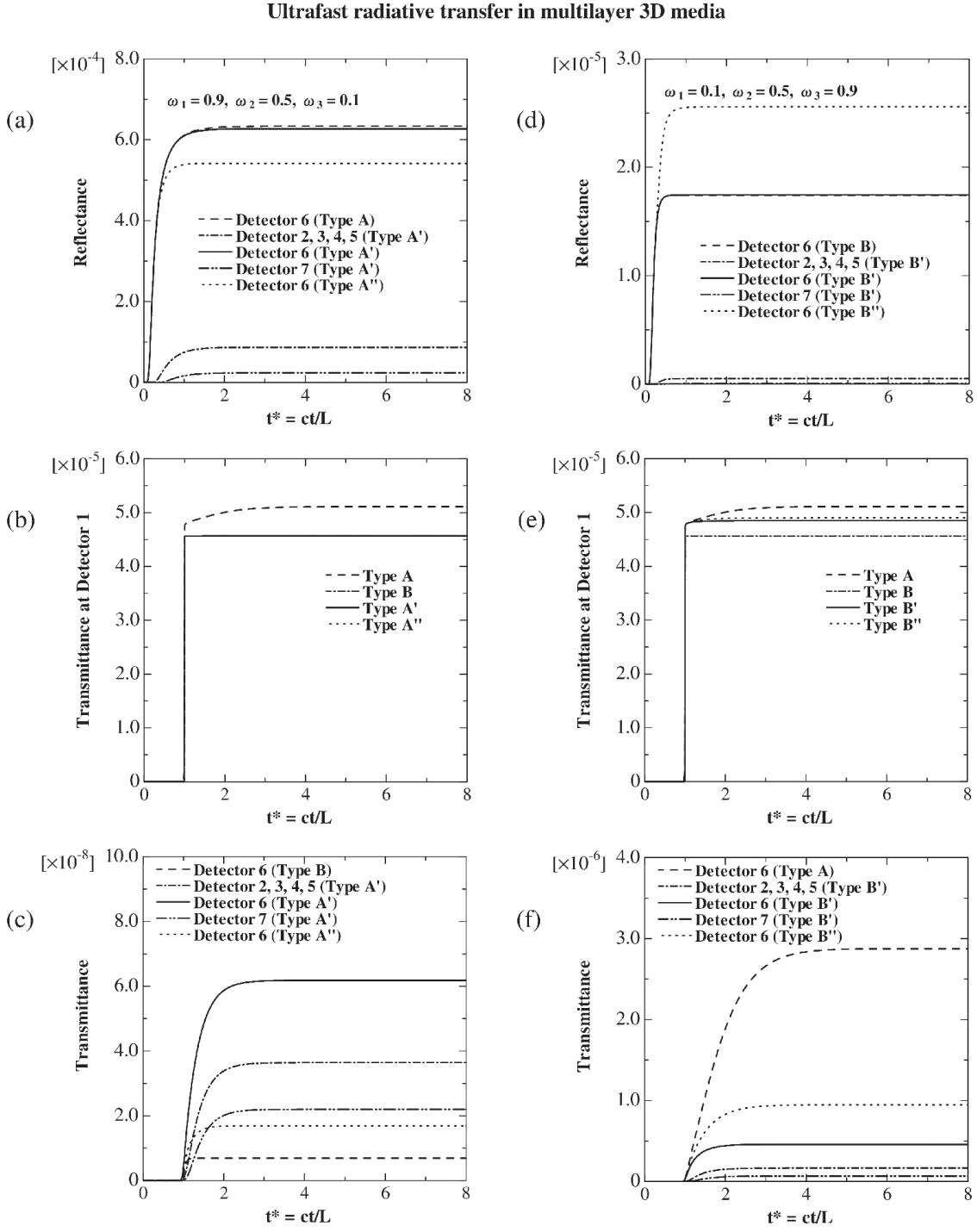

FIG. 3: Temporal profiles of the reflectance and transmittance in homogeneous and inhomogeneous participating media subjected to a single collimated unit step square pulse for Types A, A', A'' and B, B', B'' computed by the DOM

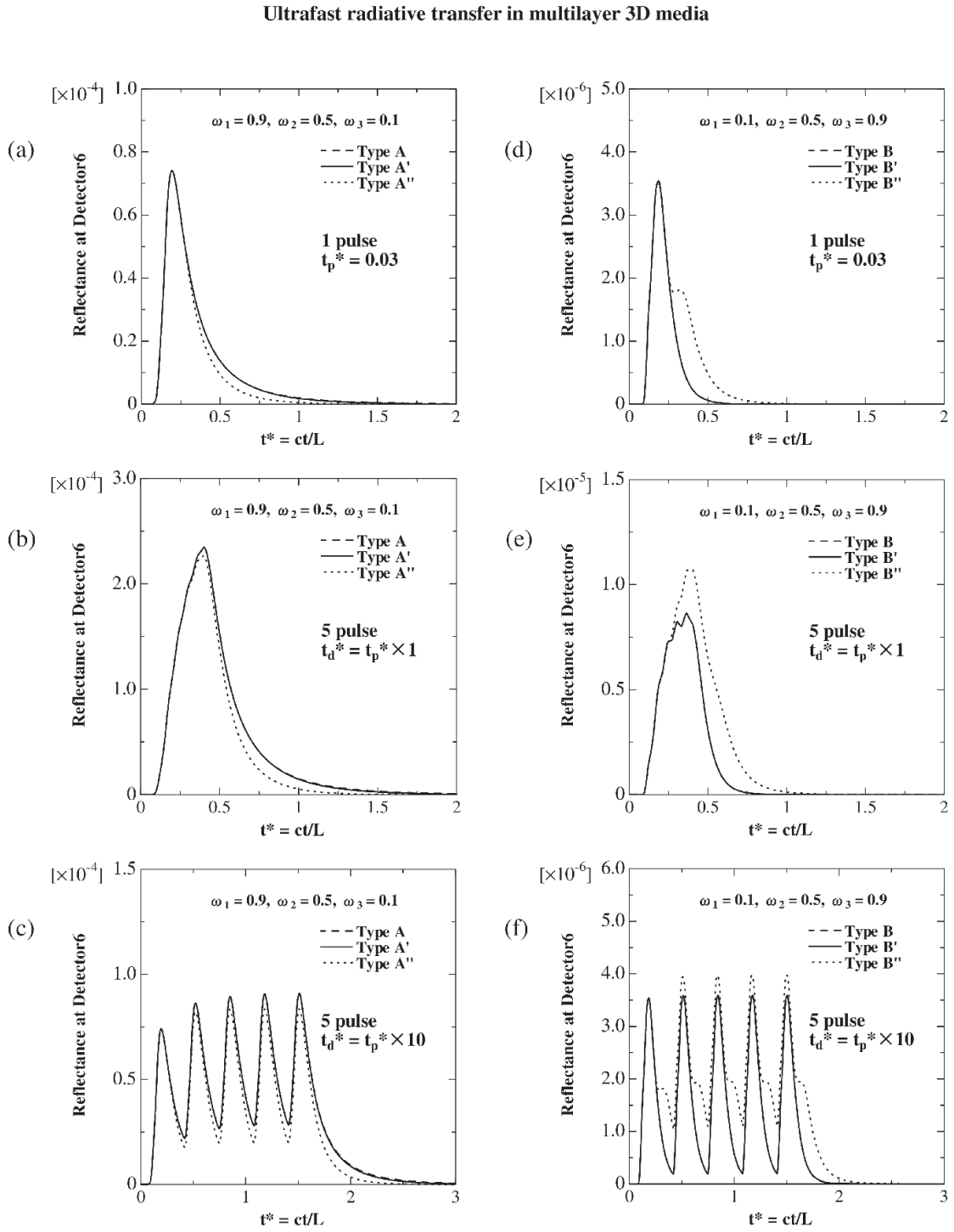

FIG. 4: Temporal profiles of the reflectance in homogeneous and inhomogeneous participating media subjected to a single collimated square pulse and a collimated square pulse train consisting of five pulses reconstructed by Duhamel's theorem for pulse width $t_p^* = 0.03$

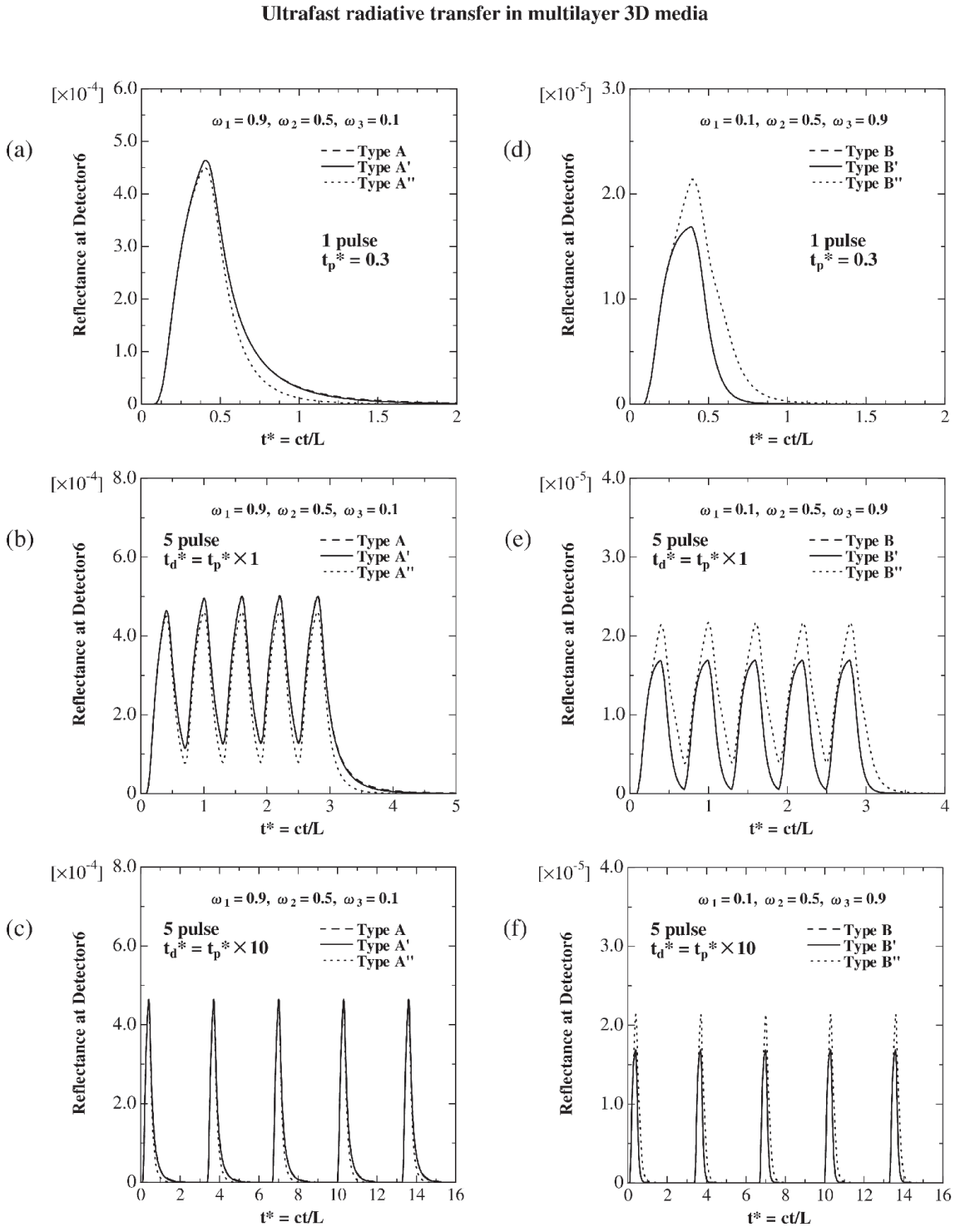

FIG. 5: Temporal profiles of the reflectance in homogeneous and inhomogeneous participating media subjected to a single collimated square pulse and a collimated square pulse train consisting of five pulses reconstructed by Duhamel's theorem for pulse width $t_p^* = 0.3$

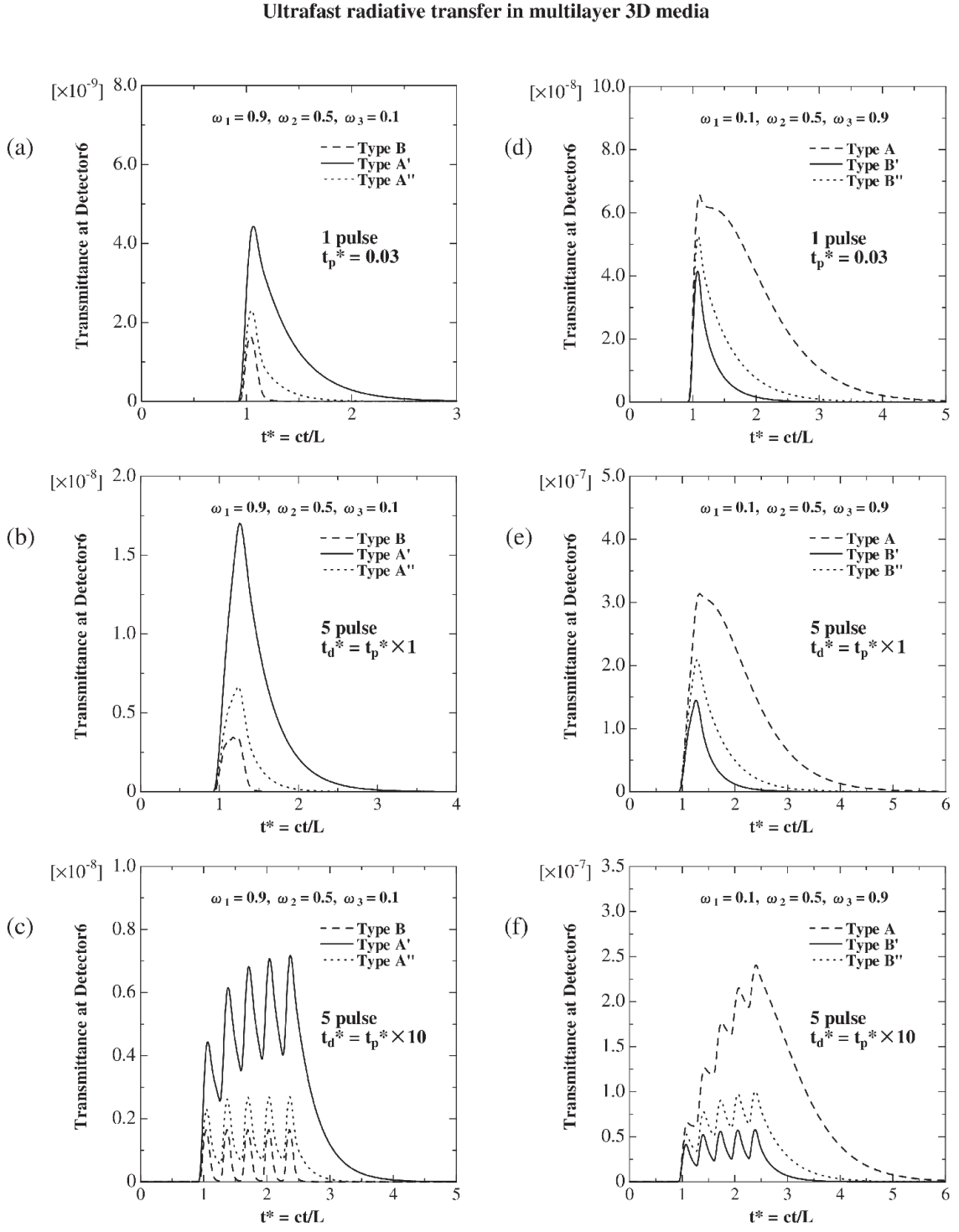

FIG. 6: Temporal profiles of the transmittance in homogeneous and inhomogeneous participating media subjected to a single collimated square pulse and a collimated square pulse train consisting of five pulses reconstructed by Duhamel's theorem for pulse width $t_p^* = 0.03$

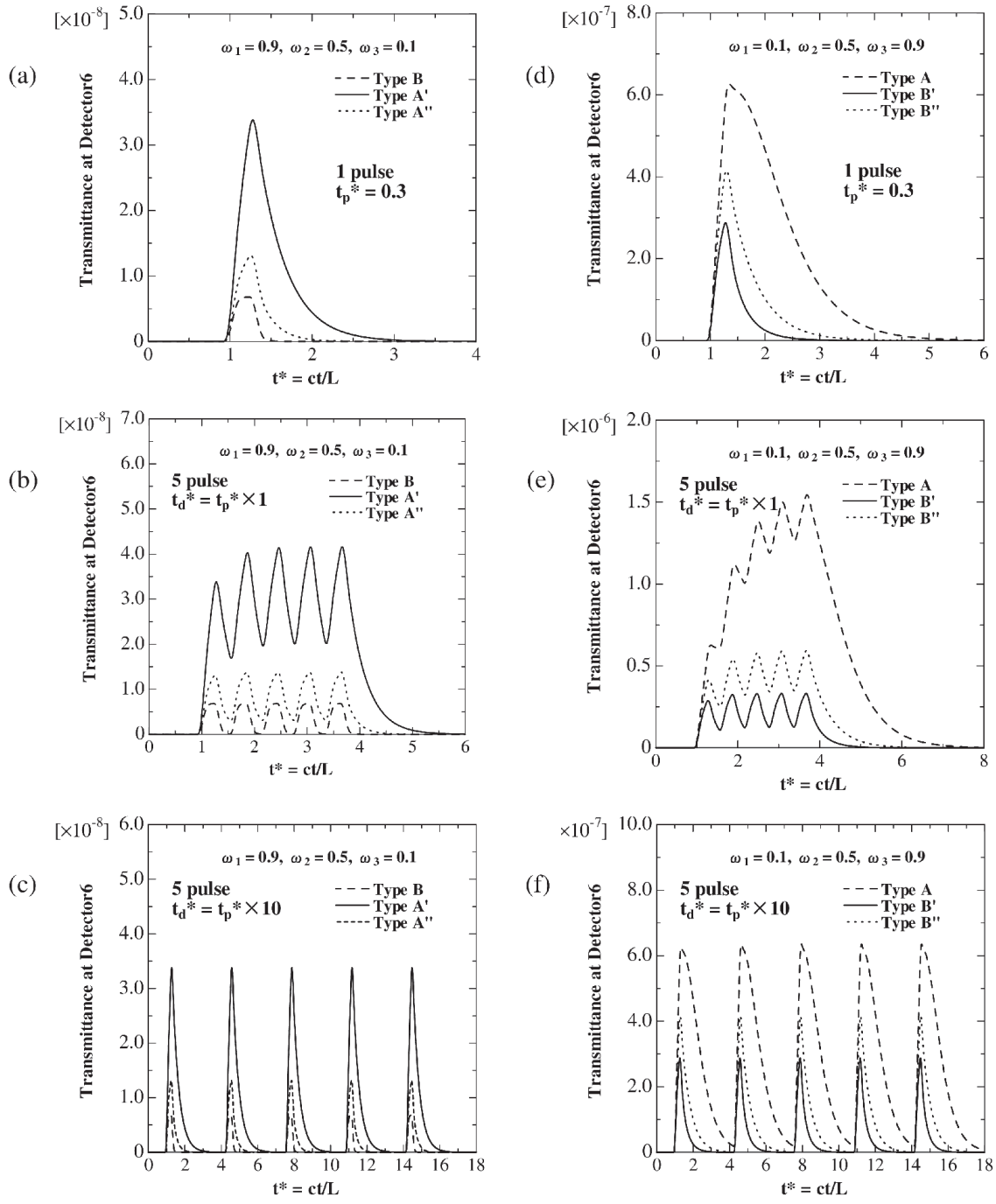

FIG. 7: Temporal profiles of the transmittance in homogeneous and inhomogeneous participating media subjected to a single collimated square pulse and a collimated square pulse train consisting of five pulses reconstructed by Duhamel's theorem for pulse width $t_p^* = 0.3$

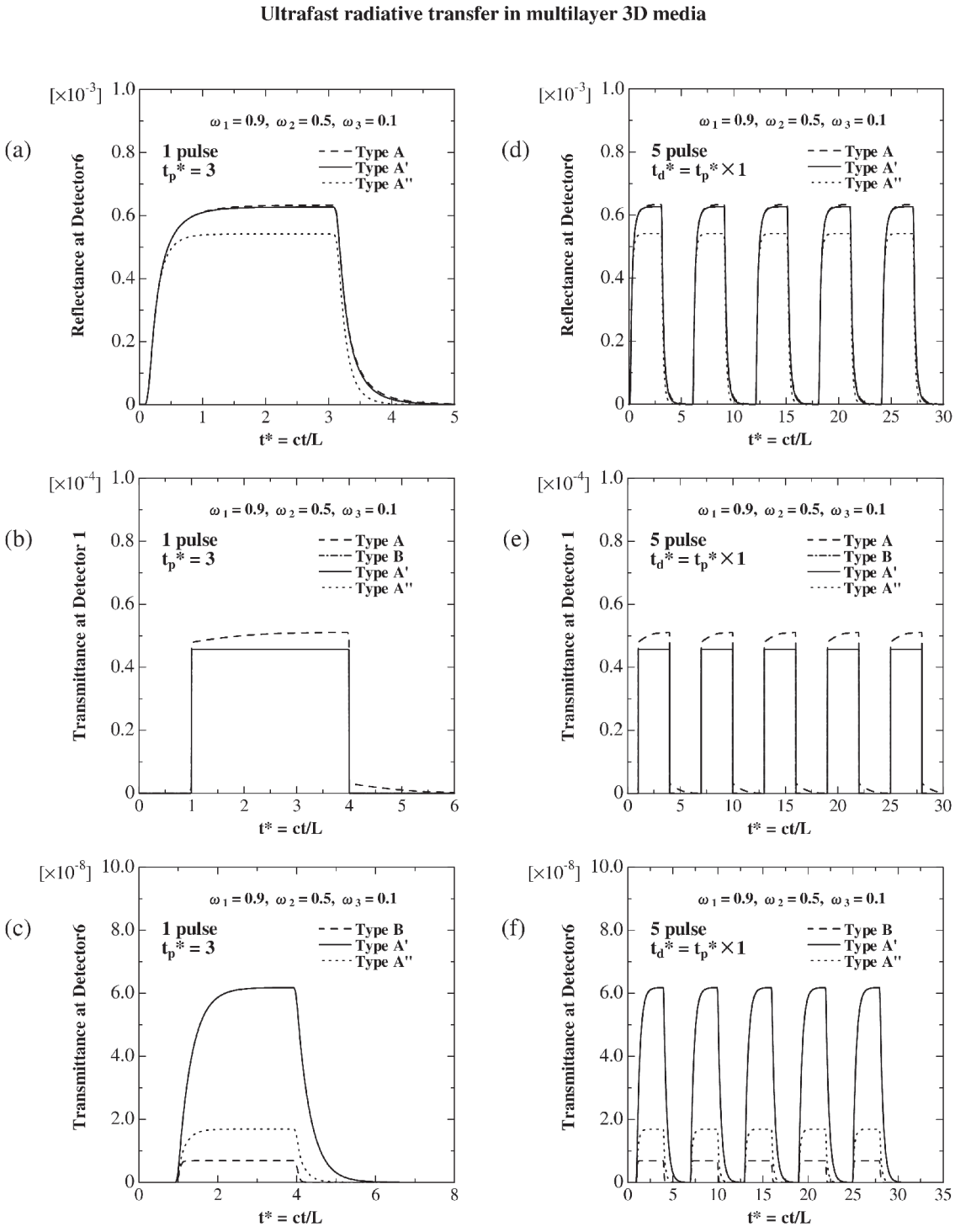

FIG. 8: Reflectance and transmittance signals in the participating medium subjected to a single collimated square pulse and a collimated square pulse train consisting of five pulses with pulse width of $t_p^* = 3$ reconstructed by Duhamel's theorem for Types A, B, A', and A'' media

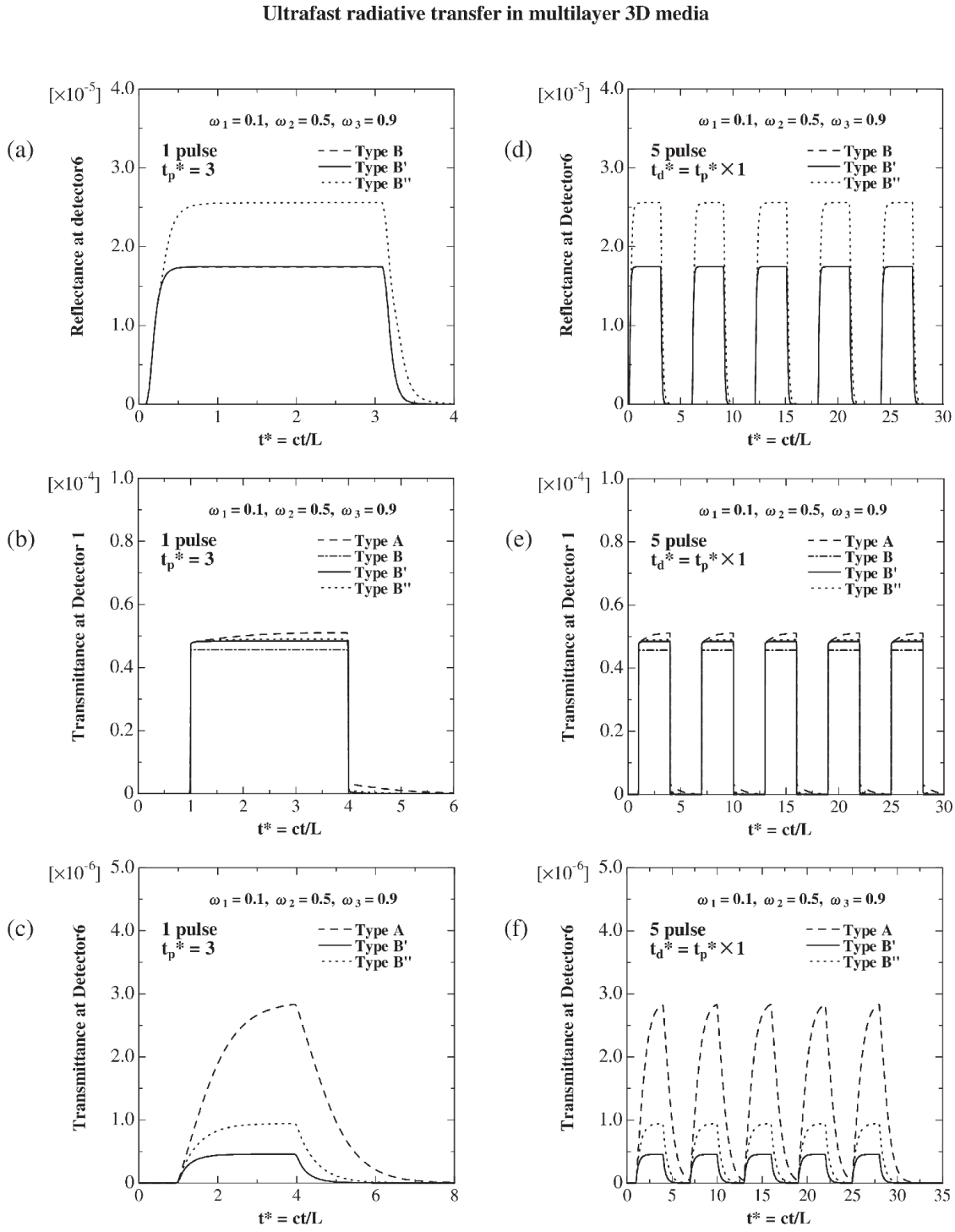

FIG. 9: Reflectance and transmittance signals in the participating medium subjected to a single collimated square pulse and a collimated square pulse train consisting of five pulses with pulse width of $t_p^* = 3$ reconstructed by Duhamel's theorem for Types A, B, B', and B'' media

greatly differed from those subjected to a pulse train shown in the rest figures. Thus, an investigation of the transport of pulse trains is needed.

When the pulse train interval between two successive pulses was short, the overlap of response from pulse train was obvious. Especially as seen in Figs. 4b and 4e, the responses of the five pulses were strongly overlapped; but the five peaks corresponding to the five pulses were still distinguishable. The overlap or superposition effect of the pulse train depends on the magnitude of the pulse broadening in the response subject to a single collimated square pulse, as well as the pulse interval. Therefore, the overlap effect of the reflectance signals for Types A, A′, and A″ is larger than that for Types B, B′, and B″ since the first layer irradiated by a pulse for Types A, A′, and A'' has a higher scattering property than that for Types B, B′, and B″. The reflectance in the homogeneous medium for Type A almost agreed with that in Type A′ composed of three inhomogeneous layers with same optical thickness, whereas those in Type A″ composed of three layers with different optical thicknesses differed from those for Types A and A′. A similar trend was also observed in the reflectance signals detected for Types B, B′, and B″. The effect of the optical property of the second layer was also clearly observed in the detected reflectance signal when the optical thickness of the first layer becomes less significant.

The corresponding figures for the transmittance signal are shown in Figs. 6 and 7. The figures in the left column are the transmittance detected by detector 6 for Types B, A′, and A″, and those in the right column are the transmittance detected by detector 6 for Types A, B′, and B″. Type B is a homogeneous medium with a high absorbing property that is identical to the third layer of Types A′ and A″. Type A is also a homogeneous medium with a high scattering property that is identical to the third layer of Types B′ and B″. From Figs. 6 and 7, it is seen that the transmittance signal detected in the medium subjected to a single square pulse greatly differed from those detected in the medium subjected to a square pulse train. With increase in the pulse train interval, the overlap effects of the transmitted pulse train gradually vanished, and the signals with five peaks were detected. The magnitude of transmitted pulse decreased with increase in the volume with optical property of $\omega = 0.1$ for Types B, A′, and A″ and with decrease in the volume with optical property of $\omega = 0.9$ for Types A, B′, and B″. The transmittance signals detected by detector 1 showed square waves similar to the irradiated pulse for any values of the pulse width and pulse train interval, indicating negligible pulse broadening at that location.

Figure 8 shows the temporal profiles of reflectance and transmittance detected by detectors 1 and 6 in the homogeneous and inhomogeneous media subjected to a single collimated square pulse and a collimated square pulse train consisting of five pulses with the pulse width of $t_p^* = 3$ for Types A, B, A′, and A″. The corresponding figures for Types A, B, B′, and B'' are shown in Fig. 9. The figures in the left column are the results of the single collimated square pulse, and those in the right column are the results of the collimated square pulse train with the pulse train interval of $t_d^* = t_p^*$. From Figs. 8 and 9, it is seen that, when the pulse train interval is long enough as compared to the pulse broadening, there is little overlap between the responses of successive pulses and the characteristics of a pulse train are similar to those of a single pulse. Here, the nondimensional pulse width and pulse train interval with $t_p^* = t_d^* = 3$ correspond to the dimensional time of 150 ps when the characteristic length L of a unit cube is 10 mm and the speed of light in the medium is 0.2 mm/ps.

6. CONCLUSIONS

We conducted transient 3D numerical computations to investigate the ultrafast radiative transfer characteristics in inhomogeneous participating media subjected to a collimated square pulse train by combining the DOM and Duhamel's superposition theorem. The efficiency of superposition was demonstrated by comparing

CPU times with and without use of superposition. Intensive studies in the homogeneous and inhomogeneous participating media subjected to a single collimated unit step square pulse, a single collimated square pulse, and a collimated square pulse train showed that (1) the magnitude of reflectance and transmittance signals depend strongly on the detecting position; (2) the reflectance signal depends strongly on the optical property of the first layer, but will be affected by the second layer if the optical thickness of the first layer becomes less significant; (3) the transmittance signals detected depends on the overall optical properties of the medium, (4) the signals detected for a single pulse greatly differed from those detected for a pulse train when the pulse interval is shorter than the pulse broadening, and (5) the signal characteristics for a pulse train can be expected from those of a single pulse when the pulse train interval is much longer than the pulse broadening.

ACKNOWLEDGMENT

M. Akamatsu acknowledges the financial support from the Murata Science Foundation for this work.

REFERENCES

Akamatsu, M. and Guo, Z., Comparison of transmitted pulse trains predicted by Duhamel's superposition theorem and direct pulse simulation in a 3-D discrete ordinates system, *Numer. Heat Transfer B*, vol. **63**, no. 3, pp. 189–203, 2013a.

Akamatsu, M. and Guo, Z., Transient prediction of radiation response in a 3-D scattering-absorbing medium subjected to a collimated short square pulse train, *Numer. Heat Transfer A*, vol. **63**, no. 5, pp. 327–346, 2013b.

Akamatsu, M. and Guo, Z., Ultrafast radiative heat transfer in three-dimensional highly-scattering media subjected to pulse train irradiation, *Numer. Heat Transfer A*, vol. **59**, no. 9, pp. 653–671, 2011.

Guo, Z and Maruyama, S., Scaling anisotropic scattering in radiative transfer in three-dimensional nonhomogeneous media, *Int. Commun. Heat Mass Transfer*, vol. **26**, no. 7, pp. 997–1007, 1999.

Guo, Z. and Hunter, B., Advances in ultrafast radiative transfer modeling and applications: A review, *Heat Transfer Res.*, vol. **44**, nos. 3–4, pp. 303–344, 2013.

Guo, Z. and Kumar, S., Discrete-ordinates solution of short-pulsed laser transport in two-dimensional turbid media, *Appl. Opt.*, vol. **40**, no. 19, pp. 3156–3163, 2001.

Guo, Z. and Kumar, S., Three-dimensional discrete ordinates method in transient radiative transfer, *J. Thermophys. Heat Transfer*, vol. **16**, no. 3, pp. 289–296, 2002.

Hebden, J. C., Veenstra, H., Dehghani, H., Hillman, E. M. C., Schweiger, M., Arridge, S. R., and Delpy, D. T., Three-dimensional time-resolved optical tomography of a conical breast phantom, *Appl. Opt.*, vol. **40**, no. 19, pp. 3278–3287, 2001.

Huang, H. and Guo, Z., Ultrashort pulsed laser ablation and stripping of freeze-dried dermis, *Lasers Med. Sci.*, vol. **25**, no. 4, pp. 517–524, 2010.

Huang, Z., Cheng, Q., Zhou, H., and Hsu, P. F., Existence of dual-peak temporal reflectance from a light pulse irradiated two-layer medium, *Numer. Heat Transfer A*, vol. **56**, no. 4, pp. 342–359, 2009.

Jiao, J. and Guo, Z., Modeling of ultrashort pulsed laser ablation in water and biological tissues in cylindrical coordinates, *Appl. Phys. B*, vol. **103**, no. 1, pp. 195–205, 2011.

Jiao, J. and Guo, Z., Thermal interaction of short-pulsed laser focused beams with skin tissues, *Phys. Med. Biol.*, vol. **54**, no. 13, pp. 4225–4241, 2009.

Kim, K, and Guo, Z., Ultrafast radiation heat transfer in laser tissue welding and soldering, *Numer. Heat Transfer A*, vol. **46**, no. 1, pp. 23–40, 2004.

Lathrop, K. D., Spatial differencing of the transport equation: Positivity vs. accuracy, *J. Comput. Phys.*, vol. **4**, no. 4, pp. 475–498, 1969.

Liu, L. H. and Hsu, P.-F., Time shift and superposition method for solving transient radiative transfer equation, *J. Quant. Spectrosc. Radiat. Transfer*, vol. **109**, no. 7, pp. 1297–1308, 2008.

Liu, L. J. and Liu, X. Y., Finite element frequency-domain diffusion approximation of transient radiative transport in planar graded index media, *Heat Transfer Res*., vol. **43**, no. 8, pp. 721–731, 2012.

Mishra, S. C., Chugh, P., Kumar, P., and Mitra, K., Development and comparison of the DTM, the DOM, and the FVM formulations for the short-pulse laser transport through a participating medium, *Int. J. Heat Mass Transfer*, vol. **49**, nos. 11–12, pp. 1820–1832, 2006.

Mishra, S. C., Muthukumaran, R., and Maruyama, S., Comparison of the thermal effects of the transport of a short-pulse laser and a multi-pulse laser through a participating medium, *Int. J. Heat Mass Transfer*, vol. **55**, nos. 21–22, pp. 5583–5596, 2012.

Modest, M. F., *Radiative Heat Transfer*, 2nd ed., New York: Academic Press, pp. 498–538, 2003.

Muthukumaran, R. and Mishra, S. C., Effect of a step short-pulse laser train on an inhomogeneous planar participating medium, *Int. Commun. Heat Mass Transfer*, vol. **35**, no. 9, pp. 1073-1078, 2008a.

Muthukumaran, R. and Mishra, S. C., Thermal signatures of a localized inhomogeneity in a 2-D participating medium subjected to an ultra-fast step-pulse laser wave, *J. Quant. Spectrosc. Radiat. Transfer*, vol. **109**, no. 5, pp. 705–726, 2008b.

Muthukumaran, R. and Mishra, S. C., Transient response of a planar participating medium subjected to a train of short-pulse radiation, *Int. J. Heat Mass Transfer*, 51(9–10), pp. 2418–2432, 2008c.

Muthukumaran, R. and Mishra, S. C., Transport of a train of short-pulse radiation of step temporal profile through a 2-D participating medium, *Int. J. Heat Mass Transfer*, vol. **51**, nos. 9–10, pp. 2282–2298, 2008d.

Muthukumaran, R., Mishra, S. C., Maruyama, S., and Mitra, K., Assessment of signals from a tissue phantom subjected to radiation sources of temporal spans of the order of a nano-, pico-, and femto-second – A numerical study, *Numer. Heat Transfer A*, vol. **60**, no. 2, pp. 154–170, 2011.

Ozisik, M. N., *Heat Conduction*, New York: Wiley, pp. 195-213, 1993.

Padhi, B. N., Rath, P., Mahapatra, S. K., and Satapathy, A. K., Short pulse collimated radiation with diffusely reflecting boundaries, *Heat Transfer Res*., vol. **42**, no. 4, pp. 301–315, 2011.

Quan, H. and Guo, Z., Fast 3-D optical imaging with transient fluorescence signals, *Opt. Express*, vol. **12**, no. 3, pp. 449–457, 2004.

Sajjadi, A. Y., Mitra, K., and Guo, Z., Thermal analysis and experiments of laser-tissue interactions: A review, *Heat Transfer Res*., vol. **44**, nos. 3–4, pp. 345–388, 2013.

Yamada, Y., Light-tissue interaction and optical imaging in biomedicine, *Annu. Rev. Heat Transfer*, vol. **6**, no. 30, pp. 1–59, 1995.

Yi, H., Ben, X., and Tan, H., Transient radiative transfer in a scattering slab considering polarization, *Opt. Express*, vol. **21**, no. 22, pp. 26693–26713, 2013.

Zhang, Y., Yi, H., and Tan, H., One-dimensional transient radiative transfer by lattice Boltzmann method, *Opt. Express*, vol. **21**, no. 21, pp. 24532–24549, 2013.

Zhang, Y., Yi, H., and Tan, H., The lattice Boltzmann method for one-dimensional transient radiative transfer in graded index gray medium, *J. Quant. Spectrosc. Radiat. Transfer*, vol. **137**, no. 3, pp. 1–12, 2014a.

Zhang, Y., Yi, H., Xie, M., and Tan, H., Short-pulsed laser transport in two-dimensional scattering media by natural element method, *J. Opt. Soc. Am. A*, vol. **31**, no. 4, pp. 818–828, 2014b.